PERGAMON

International Journal of Multiphase Flow 28 (2002) 1459–1478

International Journal of Multiphase Flow

www.elsevier.com/locate/ijmulflow

Viscous potential flow analysis of capillary instability

T. Funada [a], D.D. Joseph [b,*]

[a] Department of Digital Engineering, Numazu College of Technology, Ooka 3600, Numazu, Shizuoka, Japan
[b] Department of Aerospace Engineering and Mechanics, University of Minnesota, 110 Union Street S.E., Minneapolis, MN 55455, USA

Received 4 February 2002; received in revised form 5 May 2002

Abstract

Capillary instability of a viscous fluid cylinder of diameter D surrounded by another fluid is determined by a Reynolds number $J = VD\rho_l/\mu_l$, a viscosity ratio $m = \mu_a/\mu_l$ and a density ratio $\ell = \rho_a/\rho_l$. Here $V = \gamma/\mu_l$ is the capillary collapse velocity based on the more viscous liquid which may be inside or outside the fluid cylinder. Results of linearized analysis based on potential flow of a viscous and inviscid fluid are compared with the unapproximated normal mode analysis of the linearized Navier–Stokes equations. The growth rates for the inviscid fluid are largest, the growth rates of the fully viscous problem are smallest and those of viscous potential flow are between. We find that the results from all three theories converge when J is large with reasonable agreement between viscous potential and fully viscous flow with $J > O(10)$. The convergence results apply to two liquids as well as to liquid and gas.

Keywords: Capillary instability; Linearized Navier–Stokes equations; Viscous potential flow; Inviscid potential flow; Fully viscous flow; Stability to axisymmetric disturbances

1. Introduction

Capillary instability of a liquid cylinder of mean radius R leading to capillary collapse can be described as a neckdown due to surface tension γ in which fluid is ejected from the throat of the neck, leading to a smaller neck and greater neckdown capillary force as seen in the diagram in Fig. 1.

The dynamical theory of instability of a long cylindrical column of liquid of radius R under the action of capillary force was given by Rayleigh (1879) following earlier work by Plateau (1873)

* Corresponding author. Tel.: +1-612-625-0309; fax: +1-612-626-1558.
E-mail address: joseph@aem.umn.edu (D.D. Joseph).

0301-9322/02/$ - see front matter
PII: S0301-9322(02)00035-6

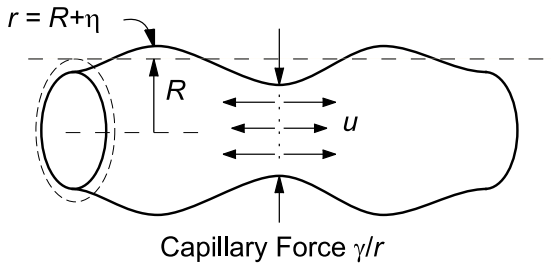

Fig. 1. Capillary instability. The force γ/r forces fluid from the throat, decreasing r leading to collapse.

who showed that a long cylinder of liquid is unstable to disturbances with wavelengths greater than $2\pi R$. Rayleigh showed that the effect of inertia is such that the wavelength λ corresponding to the mode of maximum instability is $\lambda = 4.51 \times 2R$, exceeding very considerably the circumference of the cylinder. The idea that the wavelength associated with fastest growing growth rate would become dominant and be observed in practice was first put forward by Rayleigh (1879). The analysis of Rayleigh is based on potential flow of an inviscid liquid neglecting the effect of the outside fluid. (Looking forward, we here note that it is possible and useful to do an analysis of this problem based on the potential flow of a viscous fluid.)

An attempt to account for viscous effects was made by Rayleigh (1892) again neglecting the effect of the surrounding fluid. One of the effects considered is meant to account for the forward motion of an inviscid fluid with a resistance proportional to velocity. The effect of viscosity is treated in the special case in which the viscosity is so great that inertia may be neglected. He shows that the wavelength for maximum growth is very large, strictly infinite. He says, "... long threads do not tend to divide themselves into drops at mutual distances comparable to with the diameter of the cylinder, but rather to give way by attenuation at few and distant places".

Weber (1931) extended Rayleigh's theory by considering an effect of viscosity and that of surrounding air on the stability of a columnar jet. He showed that viscosity does not alter the value of the cut-off wavenumber predicted by the inviscid theory and that the influence of the ambient air is not significant if the forward speed of the jet is small. Indeed the effects of the ambient fluid, which can be liquid or gas, might be significant in various circumstances. The problem, yet to be considered for liquid jets, is the superposition of Kelvin–Helmholtz and capillary instability.

Tomotika (1935) considered the stability to axisymmetric disturbances of a long cylindrical column of viscous liquid in another viscous fluid under the supposition that the fluids are not driven to move relative to one another. He derived the dispersion relation for the fully viscous case (his (33), our (2.17)) he solved it only under the assumption that the time derivative in the equation of motion can be neglected but the time derivative in the kinematic condition is taken into account (his (34)). This approximation leads herein to the asymptotic solution in the limit of $J \to 0$, in which the wavenumber giving maximum instability, say k_m in our notation, depends only upon the viscosity ratio $m = \mu_a/\mu_l$, where μ_l is the viscosity of liquid in another fluid of viscosity μ_a; k_m takes a maximum as $k_m R = 0.589$ at $m^{-1} = 0.28$ (which gives the critical $m_c = 3.57$), while k_m is reduced to zero as $m \to 0$ (single fluid column of high viscosity studied by Rayleigh (1892)) and $m \to \infty$ (single hollow in a fluid of high viscosity), as shown in his Fig. 2.

The parameter ℓ is important for $J \to \infty$ as is shown in Fig. 16, but not for small J (Stokes flow); inertia is not important as $J \to 0$.

The effect of viscosity on the stability of a liquid cylinder when the surrounding fluid is neglected and on a hollow (dynamically passive) cylinder in a viscous liquid was treated briefly by Chandrasekhar (1961). The parameter $\gamma R\rho_1/\mu_1^2$ which can be identified as a Reynolds number based on a velocity γ/μ_1 appears in the dispersion relation derived there.

Tomotika's problem was studied by Lee and Flumerfelt (1981) without making the approximations used by Tomotika, focusing on the elucidation of various limiting cases defined in terms of three dimensionless parameters, a density ratio, a viscosity ratio and the Ohnesorge number $Oh = \sqrt{\rho\gamma D}/\mu_1 = J^{1/2}$. They showed for various values of Oh and a fixed value of the density ratio that k_m is bounded below by Tomotika's limiting case ($Oh \to 0$) and above by the inviscid case ($Oh \to \infty$) that is independent of m; refer to their Fig. 4.

In this paper we treat the general fully viscous problem considered by Tomotika. This problem is resolved completely without approximation and is applied to 14 pairs of viscous fluids. Theories based on viscous and inviscid potential flows (VPF, IPF) are constructed and compared with the fully viscous (FVF) analysis and with each other.

It is perhaps necessary to call attention to the fact it is neither necessary or desirable to put the viscosities to zero when considering potential flows. The Navier–Stokes equations are satisfied by potential flow; the viscous term is identically zero when the vorticity is zero but the viscous stresses are not zero (Joseph and Liao, 1994). It is not possible to satisfy the no-slip condition at a solid boundary or the continuity of the tangential component of velocity and shear stress at a fluid–fluid boundary when the velocity is given by a potential. The viscous stresses enter into the viscous potential flow analysis of free surface problems through the normal stress balance (2.10) at the interface. Viscous potential flow analysis gives good approximations to fully viscous flows in cases where the shears from the gas flow are negligible; the Rayleigh–Plesset bubble is a potential flow which satisfies the Navier–Stokes equations and all the interface conditions. Joseph et al. (1999) constructed a viscous potential flow analysis of the Rayleigh–Taylor instability which can scarcely be distinguished from the exact fully viscous analysis. Similar agreements were demonstrated for viscoelastic fluids by Joseph et al. (2002). In a recent paper, Funada and Joseph (2001) analyzed Kelvin–Helmholtz instability of a plane gas–liquid layer using viscous potential flow. This problem is not amenable to analysis for the fully viscous case for several reasons identified in their paper. The study leads to unexpected results which appear to agree with experiments.

The present problem of capillary instability can be fully resolved in the fully viscous and potential flow cases and it allows us to precisely identify the limits in which different approximations work well.

2. Governing equations and dimensionless parameters

The problem formulation for the capillary instability of a viscous cylinder in another viscous fluid was formulated by Tomotika (1935). It is based on a normal mode analysis of the linearized Navier–Stokes equations. Tomotika's problem was resolved for many limiting cases by Lee and Flumerfelt (1981); they also recognized that the solution was controlled by three dimensionless parameters, $m = \mu_a/\mu_1$, $\ell = \rho_a/\rho_1$ and a Reynolds number $J = VD\rho_1/\mu_1$ where $V = \gamma/\mu_1$. A brief

review of the governing equations in dimensionless form is given below to facilitate comparison with VPF and IPF. Consider the stability of a liquid cylinder of radius $R\,(=D/2)$ with viscosity $\mu_{\rm l}$ and density $\rho_{\rm l}$ surrounded by another fluid with viscosity $\mu_{\rm a}$ and density $\rho_{\rm a}$ under capillary forces generated by interfacial tension γ. Our convention is that $\mu_{\rm l} \geqslant \mu_{\rm a}$. In the inverse problem the viscous liquid is outside. The analysis is done in cylindrical coordinates (r,θ,z) and only axisymmetric disturbances independent of θ are considered.

The governing Navier–Stokes equations and interface conditions for disturbance of the cylinder at rest are made dimensionless with the following scales

$$[\text{length},\ \text{velocity},\ \text{time},\ \text{pressure}] = [D, U, D/U, p_0]$$

where

$$p_0 = \rho_{\rm l} U^2, \quad U = \sqrt{\frac{\gamma}{\rho_{\rm l} D}}. \tag{2.1}$$

2.1. Linearized disturbance equations

The system of equations for small disturbances are given by

$$\frac{\partial u_{\rm l}}{\partial r} + \frac{u_{\rm l}}{r} + \frac{\partial w_{\rm l}}{\partial z} = 0, \tag{2.2}$$

$$\frac{\partial u_{\rm l}}{\partial t} = -\frac{\partial p_{\rm l}}{\partial r} + \frac{1}{\sqrt{J}}\left(\nabla^2 u_{\rm l} - \frac{u_{\rm l}}{r^2}\right), \tag{2.3}$$

$$\frac{\partial w_{\rm l}}{\partial t} = -\frac{\partial p_{\rm l}}{\partial z} + \frac{1}{\sqrt{J}}\nabla^2 w_{\rm l}, \tag{2.4}$$

$$\frac{\partial u_{\rm a}}{\partial r} + \frac{u_{\rm a}}{r} + \frac{\partial w_{\rm a}}{\partial z} = 0, \tag{2.5}$$

$$\ell\frac{\partial u_{\rm a}}{\partial t} = -\frac{\partial p_{\rm a}}{\partial r} + \frac{m}{\sqrt{J}}\left(\nabla^2 u_{\rm a} - \frac{u_{\rm a}}{r^2}\right), \tag{2.6}$$

$$\ell\frac{\partial w_{\rm a}}{\partial t} = -\frac{\partial p_{\rm a}}{\partial z} + \frac{m}{\sqrt{J}}\nabla^2 w_{\rm a}, \tag{2.7}$$

with

$$\nabla^2 = \frac{\partial^2}{\partial r^2} + \frac{1}{r}\frac{\partial}{\partial r} + \frac{\partial^2}{\partial z^2}. \tag{2.8}$$

The kinematic condition at the interface $r = 1/2 + \eta \approx 1/2$ (where η is the varicose displacement) is given by

$$\frac{\partial \eta}{\partial t} = u_{\rm l}, \quad \frac{\partial \eta}{\partial t} = u_{\rm a}. \tag{2.9}$$

The normal stress balance at the interface is given by

$$p_a - p_l + \frac{2}{\sqrt{J}}\frac{\partial u_l}{\partial r} - \frac{2m}{\sqrt{J}}\frac{\partial u_a}{\partial r} = \frac{\partial^2 \eta}{\partial z^2} + \frac{\eta}{R^2}. \tag{2.10}$$

The velocity normal to the interface and the velocity tangential to the interface are continuous as

$$u_l = u_a, \quad w_l = w_a. \tag{2.11}$$

The tangential stress balance at the interface is given by

$$\left(\frac{\partial u_l}{\partial z} + \frac{\partial w_l}{\partial r}\right) = m\left(\frac{\partial u_a}{\partial z} + \frac{\partial w_a}{\partial r}\right). \tag{2.12}$$

2.2. Dispersion relation for fully viscous flow (FVF)

Following Tomotika, the velocities are expressed with a stream function $\psi(r,z,t)$:

$$u = \frac{1}{r}\frac{\partial \psi}{\partial z}, \quad w = -\frac{1}{r}\frac{\partial \psi}{\partial r}, \tag{2.13}$$

and the basic variables are expressed in normal modes:

$$\psi_l = [A_1 r I_1(kr) + A_2 r I_1(k_l r)]\exp(\sigma t + \imath k z) + \text{c.c.}, \tag{2.14}$$

$$\psi_a = [B_1 r K_1(kr) + B_2 r K_1(k_a r)]\exp(\sigma t + \imath k z) + \text{c.c.}, \tag{2.15}$$

$$\eta = H\exp(\sigma t + \imath k z) + \text{c.c.}, \tag{2.16}$$

where σ is the complex growth rate and k is the wavenumber; the modified Bessel functions of the first order are denoted by I_1 for the first kind and K_1 for the second kind. Substitution of (2.14)–(2.16) into (2.11), (2.12) and (2.10) leads to the solvability condition, which is given as the dispersion relation:

$$\begin{vmatrix} I_1(kR) & I_1(k_l R) & K_1(kR) & K_1(k_a R) \\ kI_0(kR) & k_l I_0(k_l R) & -kK_0(kR) & -k_a K_0(k_a R) \\ 2k^2 I_1(kR) & (k^2 + k_l^2) I_1(k_l R) & 2mk^2 K_1(kR) & m(k^2 + k_a^2) K_1(k_a R) \\ F_1 & F_2 & F_3 & F_4 \end{vmatrix} = 0, \tag{2.17}$$

where

$$F_1 = \imath\sigma I_0(kR) + 2\imath\frac{k^2}{\sqrt{J}}\left(\frac{\mathrm{d}I_1(kR)}{\mathrm{d}(kR)}\right) - \left(\frac{1}{R^2} - k^2\right)\imath\frac{k}{\sigma}I_1(kR), \tag{2.18}$$

$$F_2 = 2\imath\frac{kk_l}{\sqrt{J}}\left(\frac{\mathrm{d}I_1(k_l R)}{\mathrm{d}(k_l R)}\right) - \left(\frac{1}{R^2} - k^2\right)\imath\frac{k}{\sigma}I_1(k_l R), \tag{2.19}$$

$$F_3 = -\imath\ell\sigma K_0(kR) + 2\imath\frac{mk^2}{\sqrt{J}}\left(\frac{\mathrm{d}K_1(kR)}{\mathrm{d}(kR)}\right), \quad F_4 = 2\imath\frac{mkk_a}{\sqrt{J}}\left(\frac{\mathrm{d}K_1(k_a R)}{\mathrm{d}(k_a R)}\right), \tag{2.20}$$

with

$$k_l = \sqrt{k^2 + \sqrt{J}\sigma}, \quad k_a = \sqrt{k^2 + \frac{\ell}{m}\sqrt{J}\sigma}. \tag{2.21}$$

For small $\sqrt{J}$, k_1 and k_a may be expanded around k up to the first order terms, which yields the expansion of (2.17)–(2.20) and the resultant dispersion relation is Eq. (34) in Tomotika's paper; that is, $\sigma =$ (a function of k and m) $\times\sqrt{J}$.

2.3. More viscous fluid outside

The equations are the same except that subscripts 'l' and 'a' are interchanged, m, ℓ, J are replaced with m', ℓ', J';

$$\left(m' = \frac{1}{m}, \quad \ell' = \frac{1}{\ell}, \quad J' = \frac{\rho_a D\gamma}{\mu_a^2}\right). \tag{2.22}$$

The capillary collapse is still controlled by the more viscous fluid $V = \gamma/\mu_l$ where μ_l is now the viscosity of the surrounding fluid. We shall index all our results with m, ℓ, J.

2.4. Dispersion relation for viscous potential flow (VPF)

The equations are the same as in Section 2.1 except that $\mathbf{u} = \nabla\phi$, $\nabla^2\phi = 0$ and the viscous terms on the right side of (2.3), (2.4), (2.6) and (2.7) are zero. The latter condition in (2.11) and the condition (2.12) which enforce a no-slip condition cannot be enforced and are omitted in the analysis of viscous potential flow.

By taking these into account in the linearized equations, the solutions are expressed as

$$\psi_l = A_1 r I_1(kr)\exp(\sigma t + \imath kz) + \text{c.c.}, \tag{2.23}$$

$$\psi_a = B_1 r K_1(kr)\exp(\sigma t + \imath kz) + \text{c.c.}, \tag{2.24}$$

$$\eta = H\exp(\sigma t + \imath kz) + \text{c.c.}, \tag{2.25}$$

for which the dispersion relation is given by

$$(\alpha_l + \ell\alpha_a)\sigma^2 + \frac{2k^2}{\sqrt{J}}(\beta_l + m\beta_a)\sigma = \left(\frac{1}{R^2} - k^2\right)k, \tag{2.26}$$

with

$$\alpha_l = \frac{I_0(kR)}{I_1(kR)}, \quad \alpha_a = \frac{K_0(kR)}{K_1(kR)}, \quad \beta_l = \alpha_l - \frac{1}{kR}, \quad \beta_a = \alpha_a + \frac{1}{kR}. \tag{2.27}$$

Solving (2.26), we get

$$\sigma = -\frac{k^2(\beta_l + m\beta_a)}{\sqrt{J}(\alpha_l + \ell\alpha_a)} \pm \sqrt{\left[\frac{k^2(\beta_l + m\beta_a)}{\sqrt{J}(\alpha_l + \ell\alpha_a)}\right]^2 + \left(\frac{1}{R^2} - k^2\right)\frac{k}{(\alpha_l + \ell\alpha_a)}}. \tag{2.28}$$

Thus instability arises in $0 < kR < 1$, for which the critical wavenumber is given by $k_c = R^{-1} = 2$. Viscous normal stresses are what produce the difference between IPF and VPF. This difference is small when k is small and large for k near to one (see Figs. 2–8).

For large $\sqrt{J}$, (2.28) reduces to

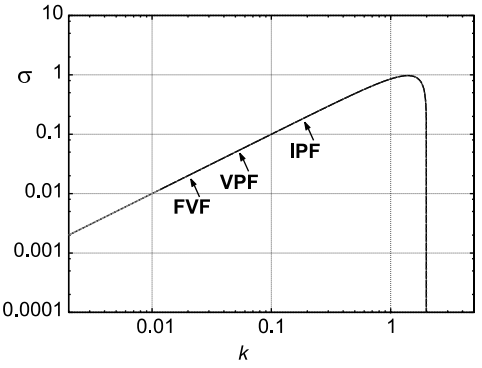

Fig. 2. The growth rate σ vs. k for case 1, mercury in air.

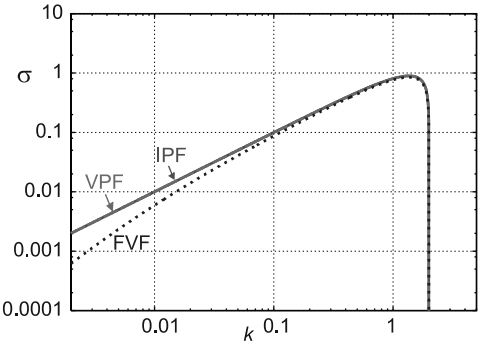

Fig. 3. The growth rate σ vs. k for case 5, water in benzene.

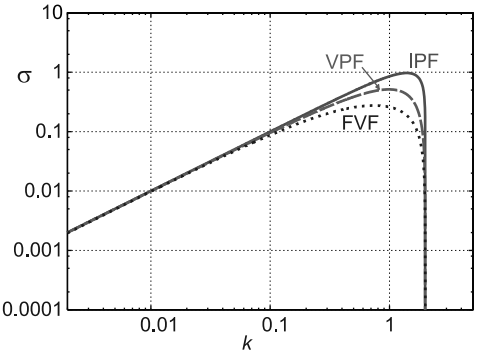

Fig. 4. The growth rate σ vs. k for case 8, glycerine in air.

$$\sigma = \pm\sqrt{\left(\frac{1}{R^2} - k^2\right)\frac{3k}{(\alpha_l + \ell\alpha_a)}}, \tag{2.29}$$

which is just the solution in the IPF, giving for instability a maximum growth rate $\sigma_m = \sigma(k_m)$ with the associated wavenumber k_m. When J is not too small, (2.28) reduces to (2.29) in the limit

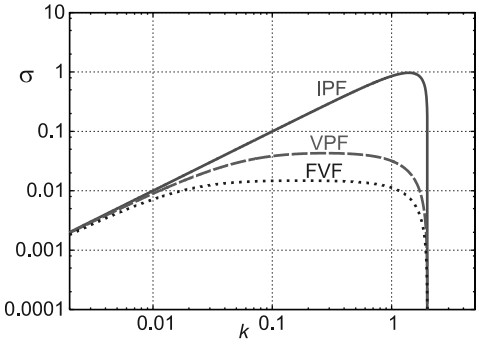

Fig. 5. The growth rate σ vs. k for case 11, SO10000 in air.

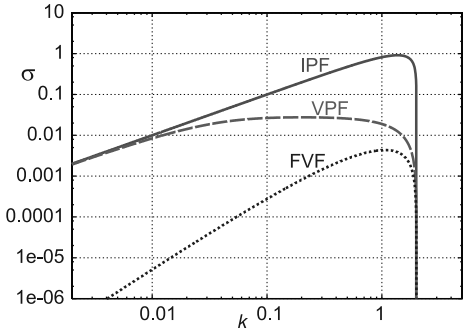

Fig. 6. The growth rate σ vs. k for case 12, goldensyrup in BBoil.

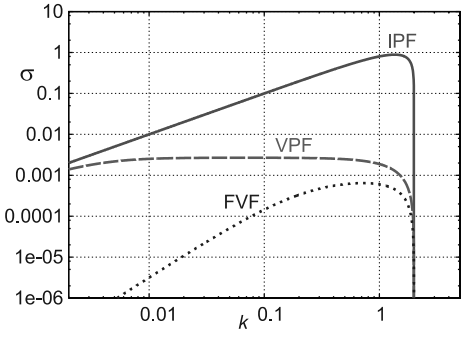

Fig. 7. The growth rate σ vs. k for case 14, tar pitch mixture in goldensyrup.

$k \to 0$; in this case the normal viscous stresses disappear and σ of VPF has the same asymptotic form as IPF.

For small $\sqrt{J}$, (2.28) for instability is reduced to

$$\sigma = \frac{1}{2}\left(\frac{1}{R^2} - k^2\right)\frac{\sqrt{J}}{k(\beta_1 + m\beta_a)}, \tag{2.30}$$

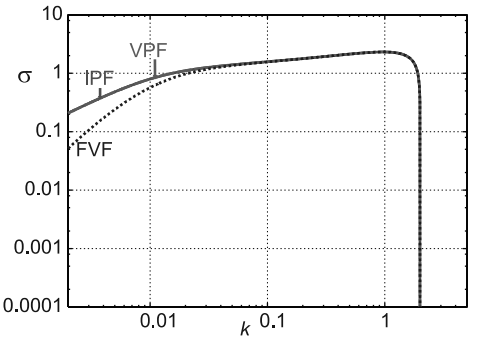

Fig. 8. The growth rate σ vs. k for case 15 (inverse), air in mercury; $k_{mI} = k_{mV} = k_{mF} = 0.9696$, $\sigma_{mI} = 2.319$, $\sigma_{mV} = 2.318$, $\sigma_{mF} = 2.317$, for which $\sigma_{mV}/\sigma_{mI} = 0.9996$ and $\sigma_{mV}/\sigma_{mF} = 1.000$.

which is another asymptotic solution in $J \to 0$ and is in good agreement with the curves of maximum growth rate σ_m of VPF in Figs. 11–15. Therefore we find that VPF bridges two asymptotic solutions, one is given by (2.29) when $J \to \infty$ and the other is given by (2.30) in the limit of $J \to 0$; the latter is not included in IPF. In the limit of $k \to 0$, (2.30) is then reduced to $\sigma = \sqrt{J}/(1+m)$, which changes monotonically with increasing m. This aspect is different from that of FVF (where k_m for small $\sqrt{J}$ has a maximum with respect to m and is reduced to 0 for $m \to 0$ and $m \to \infty$; refer to Tomotika (1935) and Lee and Flumerfelt (1981)).

Around the maximum growth rate, $\sigma_m = \sigma(k_m)$ and $d\sigma_m/dk_m = 0$, we have an expansion of σ:

$$\sigma(k) = \sigma_m + \frac{1}{2}\frac{d^2\sigma_m}{dk_m^2}(k - k_m)^2 + \cdots, \tag{2.31}$$

thus σ_m, k_m and the curvature $d^2\sigma_m/dk_m^2$ may be used to compare the results of VPF, FVF and IPF.

3. Growth rate curves, σ vs. k

Growth rate curves were computed for 14 fluid pairs; 'l', 'a' are listed in Table 1.

In Table 2 we list the 28 values of dimensionless parameters needed to calculate growth rates for fully viscous flow; 14 when the more viscous liquid is inside and an additional 14 when the more viscous liquid is outside. Growth rate curves σ vs. k for the 14 fluids listed in Table 1 are given in Figs. 2–7. The inverse case, with the viscous fluid outside, is plotted in Fig. 8. There are three curves in each figure belonging to fully viscous, viscous potential and IPF. The curves have a universal order with the highest growth given by IPF and the lowest growth rates by FVF. Long waves are more stable for FVF than VPF (especially when m is close to the critical; see Figs. 3,6–8), but the peak values are very close (see Fig. 7, where $\left|d^2\sigma_{mV}/dk_{mV}^2\right|$ is small).

Table 3 lists the maximum growth rate and the wavenumber of maximum growth for fully viscous and viscous potential flow. We measure the agreement by monitoring the ratio of maximum growth rates σ_{mV}/σ_{mF} and the ratio of the maximizing wavenumbers. The agreement is good when these ratios are nearly one. Table 3 shows very good agreements for high Reynolds numbers greater than $O(10^4)$ and reasonable agreement for Reynolds numbers greater than O(1).

Table 1
Fluid pairs for study of capillary instability when the viscous fluid is inside

No.	Material (fluid l–fluid a)	ρ_l (kg m^{-3})	μ_l (kg/m s)	ρ_a (kg m^{-3})	μ_a (kg/m s)	γ (N/m)
1	Mercury–air	13500	0.00156	1.2	1.8×10^{-5}	0.4821
2	Mercury–water	13500	0.00156	1000	0.001	0.375
3	Water–air	1000	0.001	1.2	1.8×10^{-5}	0.0728
4	Benzene–air	860	0.00065	1.2	1.8×10^{-5}	0.02886
5	Water–benzene	1000	0.001	860	0.00065	0.0328
6	SO100–air	969	0.1	1.2	1.8×10^{-5}	0.021
7	Glycerine–mercury	1257	0.782	13500	0.00156	0.375
8	Glycerine–air	1257	0.782	1.2	1.8×10^{-5}	0.0634
9	Oil–air	879.8	0.483	1.3	1.85×10^{-5}	0.0315
10	Goldensyrup–CC4 and paraffin	1400	11.0	1600	0.0034	0.023
11	SO10000–air	969	10.0	1.2	1.8×10^{-5}	0.021
12	Goldensyrup–BBoil	1400	11.0	900	6.0	0.017
13	Goldensyrup–Black lubrication oil	1400	11.0	850	10.0	0.008
14	Tar pitch mixture–goldensyrup	1400	200.0	1400	11.0	0.023

Density (kg m^{-3}), viscosity (kg/m s) and interfacial tension (N/m). An additional 14 pairs numbered from 15–28 are obtained by inverting 1–14 so that the viscous fluid is outside; for example, 15 is air–mercury. These 28 fluid pairs are the data base for this paper.

Table 2
Dimensionless parameters $\ell = \rho_a/\rho_l$, $m = \mu_a/\mu_l$ and $J = \rho\gamma D/\mu^2$ is a Reynolds number based on the maximum viscosity, which is the viscosity μ_l listed in Table 1

No.	ℓ	m	No.	ℓ	m	J
1	8.889E−05	1.154E−02	15	1.125E+04	8.667E+01	2.674E+07
2	7.407E−02	6.410E−01	16	1.350E+01	1.560E+00	2.080E+07
3	1.200E−03	1.800E−02	17	8.333E+02	5.556E+01	7.280E+05
4	1.395E−03	2.769E−02	18	7.167E+02	3.611E+01	5.874E+05
5	8.600E−01	6.500E−01	19	1.163E+00	1.538E+00	3.280E+05
6	1.238E−03	1.800E−04	20	8.075E+02	5.556E+03	2.035E+01
7	1.074E+01	1.995E−03	21	9.311E−02	5.013E+02	7.708E+00
8	9.547E−04	2.302E−05	22	1.048E+03	4.344E+04	1.303E+00
9	1.478E−03	3.830E−05	23	6.768E+02	2.611E+04	1.188E+00
10	1.143E+00	3.091E−04	24	8.750E−01	3.235E+03	2.661E−03
11	1.238E−03	1.800E−06	25	8.075E+02	5.556E+05	2.035E−03
12	6.429E−01	5.455E−01	26	1.556E+00	1.833E+00	1.967E−03
13	6.071E−01	9.091E−01	27	1.647E+00	1.100E+00	9.256E−04
14	1.000E+00	5.500E−02	28	1.000E+00	1.818E+01	8.050E−06

Entries 15–28 are for cases in which μ_l and ρ_l are for the outside fluid.

We call the readers attention to the fact that the agreements between fully viscous and viscous potential flow are good when J is large, even the fluid when the pairs are two liquids. This result is in apparent disagreement with the notion that such agreements are somehow associated with the

Table 3
Maximum growth rate and the associated wavenumber ratios indexed by J; cases 1–14 are viscous fluid inside

No.	J	k_{mV}	σ_{mV}	k_{mF}	σ_{mF}	k_{mV}/k_{mF}	σ_{mV}/σ_{mF}
1	2.6744E+07	1.3957E+00	9.7090E−01	1.3957E+00	9.7048E−01	1.0000E+00	1.0004E+00
2	2.0803E+07	1.3894E+00	9.6337E−01	1.3894E+00	9.5517E−01	1.0000E+00	1.0086E+00
3	2.0803E+07	1.3957E+00	9.6975E−01	1.3894E+00	9.6706E−01	1.0045E+00	1.0028E+00
4	7.2800E+05	1.3957E+00	9.6958E−01	1.3894E+00	9.6643E−01	1.0045E+00	1.0033E+00
5	5.8745E+05	1.3585E+00	8.9325E−01	1.3524E+00	8.4918E−01	1.0045E+00	1.0519E+00
6	3.2800E+05	1.2416E+00	7.8900E−01	1.0898E+00	5.9326E−01	1.1393E+00	1.3299E+00
7	3.1834E+04	1.0704E+00	4.7575E−01	9.9608E−01	3.4141E−01	1.0746E+00	1.3935E+00
8	2.0349E+01	9.8716E−01	5.1382E−01	7.4027E−01	2.7489E−01	1.3335E+00	1.8692E+00
9	1.3032E+00	9.7832E−01	5.0282E−01	7.3035E−01	2.6577E−01	1.3395E+00	1.8920E+00
10	1.1880E+00	2.9710E−01	4.8735E−02	2.7033E−01	1.6553E−02	1.0990E+00	2.9442E+00
11	4.2500E−03	2.7772E−01	4.2951E−02	1.7242E−01	1.4812E−02	1.6108E+00	2.8998E+00
12	2.0349E−03	2.0181E−01	2.7576E−02	1.0608E+00	4.3485E−03	1.9024E−01	6.3414E+00
13	6.8000E−04	1.4468E−01	1.5550E−02	1.1146E+00	2.2753E−03	1.2980E−01	6.8343E+00
14	8.0500E−06	6.7356E−02	2.6807E−03	7.1733E−01	6.4485E−04	9.3898E−02	4.1571E+00

The ratios are nearly one, indicating agreement between FVF and VPF when J is large.

Table 4
Maximum growth rate and wavenumber ratios for VPF and IPF when the viscous liquid is inside (No. 1–14)

No.	k_{mI}	σ_{mI}	k_{mV}	σ_{mV}	k_{mV}/k_{mI}	σ_{mV}/σ_{mI}
1	1.3957E+00	9.7110E−01	1.3957E+00	9.7090E−01	1.0000E+00	9.9979E−01
2	1.3894E+00	9.6377E−01	1.3894E+00	9.6337E−01	1.0000E+00	9.9958E−01
3	1.3957E+00	9.7099E−01	1.3957E+00	9.6975E−01	1.0000E+00	9.9873E−01
4	1.3957E+00	9.7097E−01	1.3957E+00	9.6958E−01	1.0000E+00	9.9857E−01
5	1.3585E+00	8.9590E−01	1.3585E+00	8.9325E−01	1.0000E+00	9.9704E−01
6	1.3957E+00	9.7098E−01	1.2416E+00	7.8900E−01	8.8965E−01	8.1258E−01
7	1.1924E+00	5.5735E−01	1.0704E+00	4.7575E−01	8.9769E−01	8.5361E−01
8	1.3957E+00	9.7101E−01	9.8716E−01	5.1382E−01	7.0731E−01	5.2916E−01
9	1.3957E+00	9.7096E−01	9.7832E−01	5.0282E−01	7.0098E−01	5.1786E−01
10	1.3463E+00	8.7508E−01	2.9710E−01	4.8735E−02	2.2067E−01	5.5692E−02
11	1.3957E+00	9.7098E−01	2.7772E−01	4.2951E−02	1.9899E−01	4.4235E−02
12	1.3646E+00	9.1304E−01	2.0181E−01	2.7576E−02	1.4788E−01	3.0202E−02
13	1.3708E+00	9.1596E−01	1.4468E−01	1.5550E−02	1.0554E−01	1.6977E−02
14	1.3524E+00	8.8539E−01	6.7356E−02	2.6807E−03	4.9804E−02	3.0277E−03

behavior of boundary layers at gas–liquid surfaces (see Section 6) and not with boundary layers at liquid–liquid surfaces.

In Table 4 we give the growth rate ratios and associated wavenumber ratios for VPF and IPF.

4. Maximum growth rates and wavenumbers, σ_m and k_m vs. $\sqrt{J}$

The growth rate curves σ vs. k depend only on three control parameters ℓ, m and J. The dimensionless description allows for maximum generality. We show how σ_m and k_m from FVF vary with $\sqrt{J}$ for different values of ℓ and m in Figs. 9 and 10.

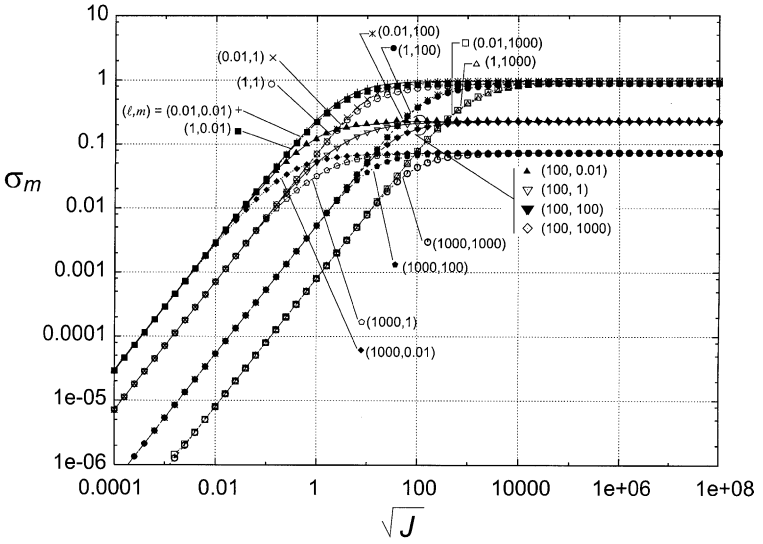

Fig. 9. Maximum growth rate σ_m vs. $\sqrt{J}$ for various values of ℓ and m in the fully viscous case.

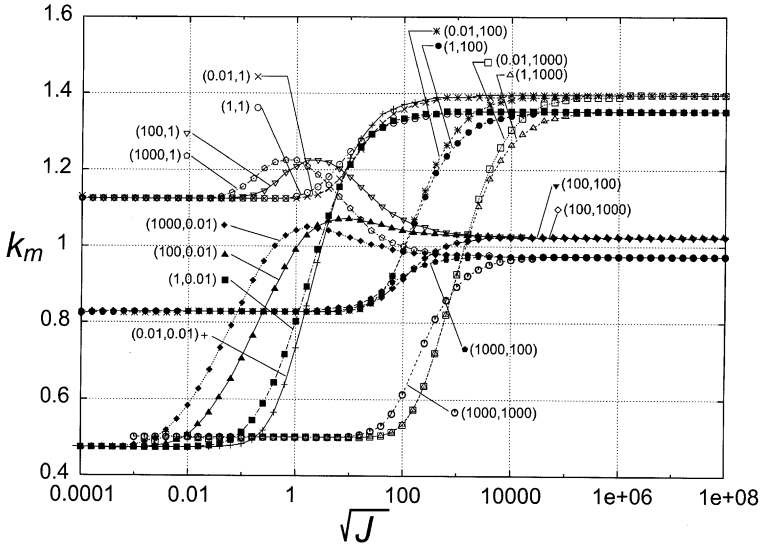

Fig. 10. Wavenumber k_m vs. $\sqrt{J}$ for the values of ℓ and m for FVF. The existence of a maximum value of k_m at values of J near 1 for certain values of ℓ and m is noteworthy. For small $\sqrt{J}$, k_m has a maximum with respect to m. For large $\sqrt{J}$, all theories collapse to IPF which does not depend on the viscosity ratio m but does depend on the density ratio ℓ.

For large $\sqrt{J}$, the maximum growth rate in Fig. 9 depends only upon ℓ as expected just by IPF. For small $\sqrt{J}$, the maximum growth rate is proportional to $\sqrt{J}$ and is shifted by m, which is evaluated by Tomotika's (34). Eq. (2.17) includes these two asymptotic solutions.

Corresponding to Fig. 9, k_m changes with $\sqrt{J}$ as in Fig. 10. For large $\sqrt{J}$, k_m is evaluated by IPF ($0.9696 \leqslant k_m \leqslant 1.396$, for which refer to (5.2) and (5.3) and Fig. 16(b)). For small $\sqrt{J}$, k_m has a maximum with respect to m and is reduced to 0 for $m \to 0$ and $m \to \infty$; note that $k_m = 1.178$ at $m_c = 3.57$, thus $0 < k_m \leqslant 1.178$. The existence of a maximum value of k_m at values of J near 1 for certain values of ℓ and m is noteworthy.

In Figs. 11–15 we plotted the peak values σ_m and the corresponding wavenumber k_m vs. $\sqrt{J}$ for fixed values of ℓ and m which are given in Table 2. We can find the two asymptotic solutions, one is given by IPF for large $\sqrt{J}$ and the other is given for small $\sqrt{J}$; (2.30) for VPF and Tomotika's (34) for FVF. The maximum growth rate σ_m and k_m for IPF do not depend on J and m and appear as the highest flat value. The smallest growth rate is for FVF.

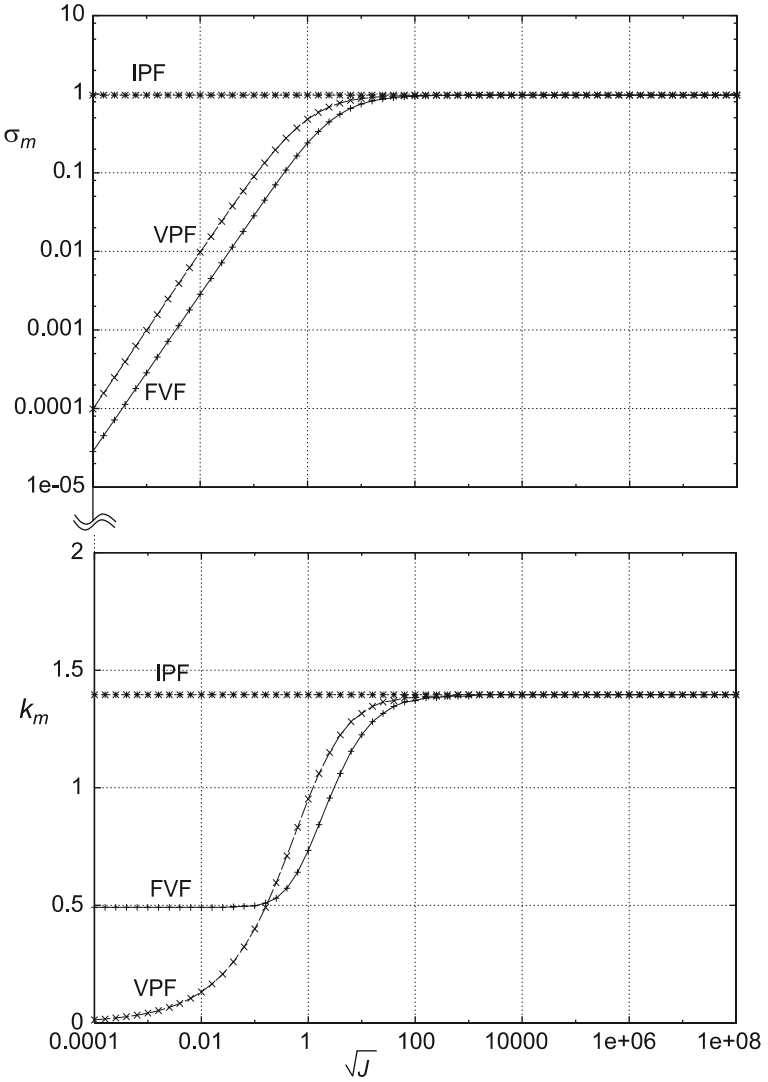

Fig. 11. σ_m and k_m vs. $\sqrt{J}$ for values of $(\ell, m) = (8.889 \times 10^{-5}, 1.154 \times 10^{-2})$ for mercury in air.

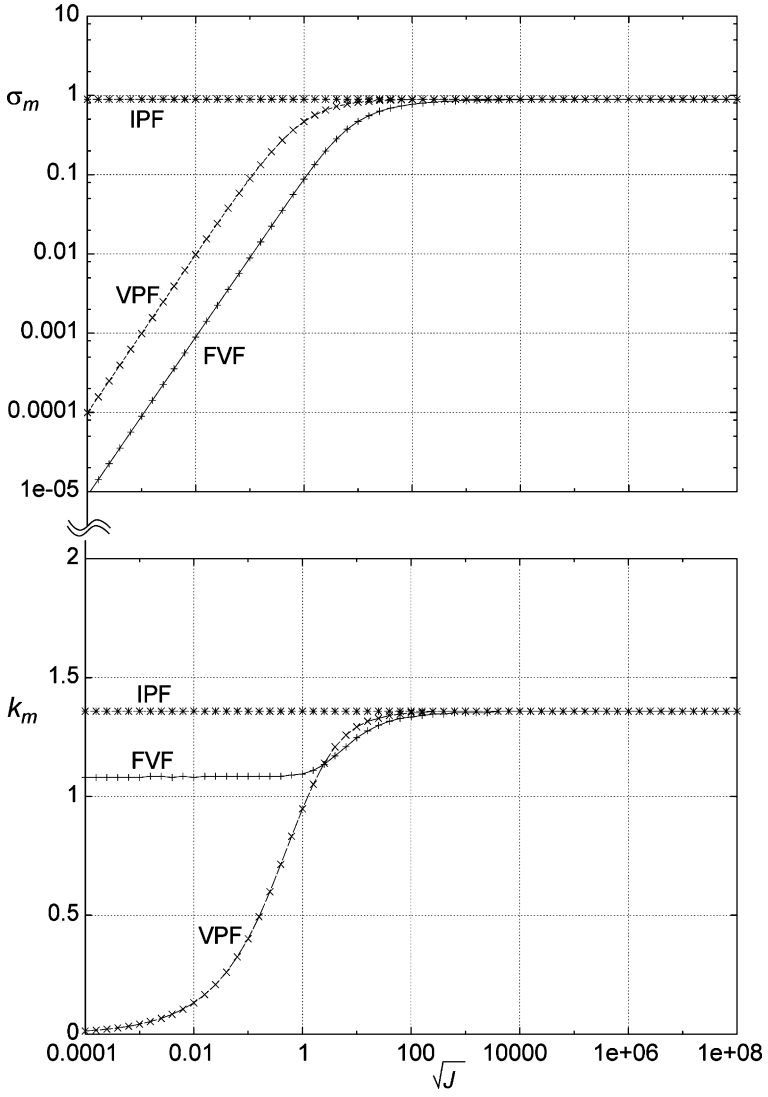

Fig. 12. σ_{m} and k_{m} vs. $\sqrt{J}$ for values of $(\ell, m) = (8.600 \times 10^{-1}, 6.500 \times 10^{-1})$ for water in benzene.

5. σ_{mI} vs. k_{m} for inviscid potential flow (IPF)

For IPF, the growth rate σ_{I} (based upon the time scale $T_{\mathrm{l}} = D/U_{\mathrm{l}}$, $U_{\mathrm{l}} = \sqrt{\gamma/(\rho_{\mathrm{l}} D)}$, $\ell = \rho_{\mathrm{a}}/\rho_{\mathrm{l}}$ and $R = 1/2$) is expressed as

$$\sigma_{\mathrm{I}} = \sqrt{\left(\frac{1}{R^2} - k^2\right)\frac{k}{(\alpha_{\mathrm{l}} + \ell\alpha_{\mathrm{a}})}}. \tag{5.1}$$

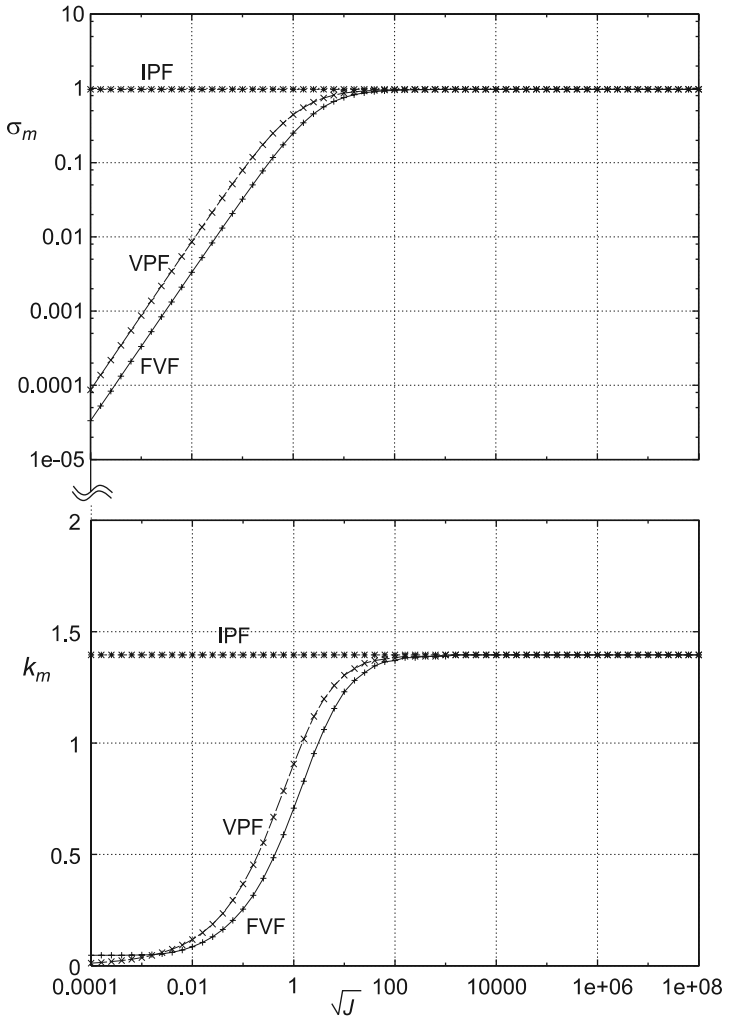

Fig. 13. σ_{m} and k_{m} vs. $\sqrt{J}$ for values of $(\ell, m) = (1.238 \times 10^{-3}, 1.800 \times 10^{-6})$ for SO10000 in air.

For small ℓ, this reduces to $\sigma_{\mathrm{I}} = \sqrt{((1/R^2) - k^2)(k/\alpha_\ell)}$, while for large ℓ, it reduces to $\sigma_{\mathrm{I}} = \sqrt{((1/R^2) - k^2)(k/\ell\alpha_{\mathrm{a}})}$. Thus, combination of the results shown in Fig. 16 leads to asymptotic forms of the maximum growth rate σ_{mI}:

$$\sigma_{\mathrm{mI}} = \begin{cases} 0.971 \text{ at } k_{\mathrm{mI}} = 1.39 \quad \text{for } \ell \ll 1, \\ 2.319 \times \ell^{-1/2} \text{ at } k_{\mathrm{mI}} = 0.969 \quad \text{for } \ell \gg 1. \end{cases} \tag{5.2}$$

If the fluid of density ρ_{l} is outside and ρ_{a} inside, then $T_{\mathrm{a}} = D/U_{\mathrm{a}}$, $\ell' = 1/\ell$ and the subscript 'a' and 'l' are interchanged in (5.1), for which we find that

$$\sigma_{\mathrm{mI}} = \begin{cases} 2.319 \text{ at } k_{\mathrm{mI}} = 0.9696 \quad \text{for } \ell' \ll 1, \\ 0.9711 \times \ell'^{-1/2} \text{ at } k_{\mathrm{mI}} = 1.396 \quad \text{for } \ell' \gg 1. \end{cases} \tag{5.3}$$

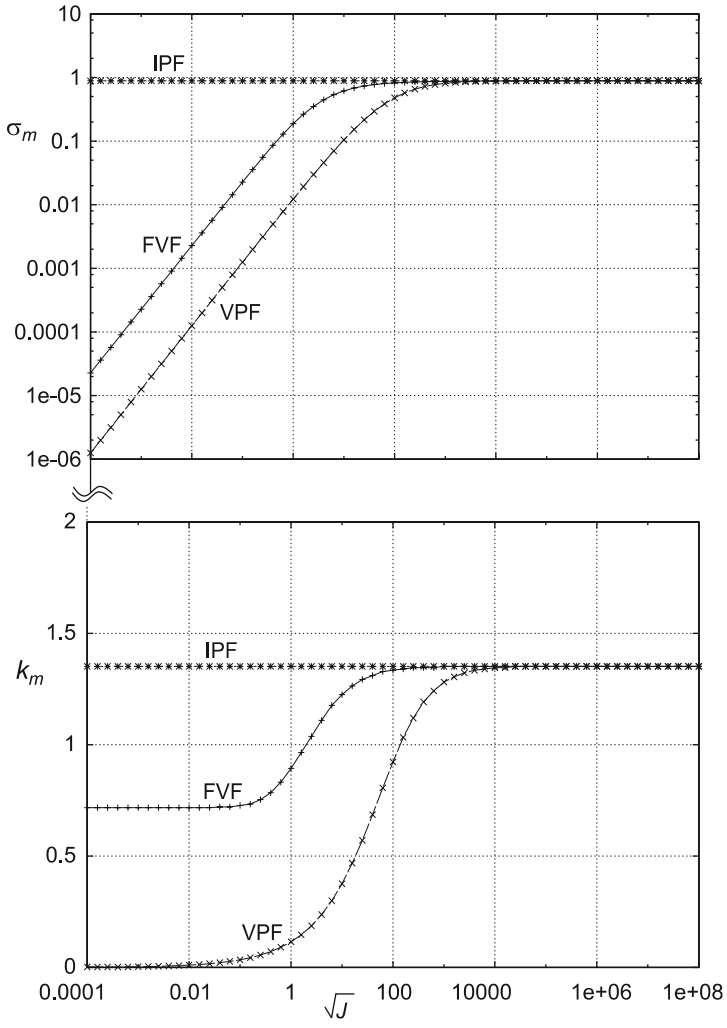

Fig. 14. σ_m and k_m vs. $\sqrt{J}$ for values of $(\ell, m) = (1.000, 5.500 \times 10^{-2})$ for tar pitch mixture in goldensyrup.

The asymptotic form (5.2) and (5.3) are shown as dashed lines in Fig. 16. The cross point in Fig. 16(a) is given by $\ell^{1/2} = 2.319/0.971$, which gives the critical value $\ell_c = 5.70$ ($\ell'_c = 1/\ell_c = 0.175$). This may be used to evaluate σ_m, though the corresponding wavenumber k_m changes in the range wider than $0.175 < \ell < 5.70$. It is stressed, however, that when J is large VPF has two structures as in IPF.

6. Conclusions and discussion

We studied capillary instability of a fluid cylinder of viscosity μ_l in a fluid with viscosity μ_a; the fluids may be liquid or gas. The problem is completely characterized by three numbers: a viscosity

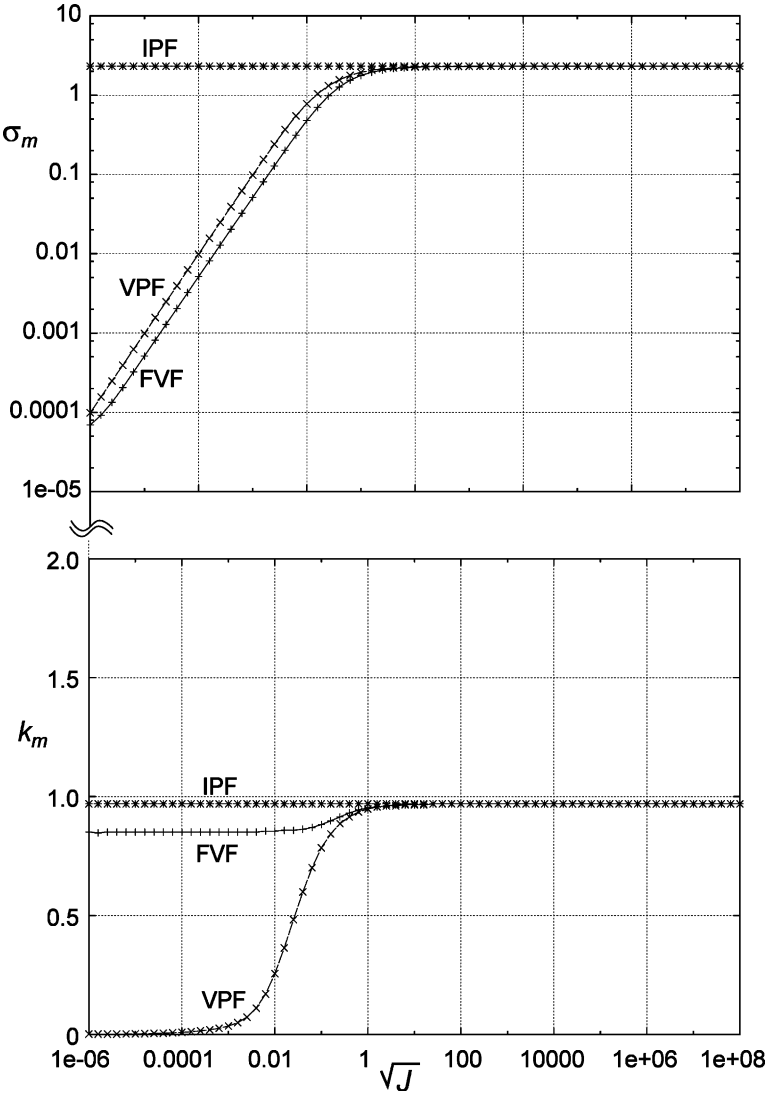

Fig. 15. σ_{m} and k_{m} vs. $\sqrt{J}$ for values of $(\ell, m) = (1.125 \times 10^4, 8.667 \times 10^1)$ for air in mercury.

ratio $m = \mu_{\mathrm{a}}/\mu_{\mathrm{l}}$, a density ratio $\ell = \rho_{\mathrm{a}}/\rho_{\mathrm{l}}$ and by a Reynolds number $J = \rho_\ell \gamma D/\mu_{\mathrm{l}}^2$ based on a collapse velocity γ/μ_{l} where μ_{l} and ρ_{l} are for the more viscous of the two fluids. The goal of the present study is to evaluate the utility of viscous potential flow as an approximation to the unapproximated viscous problem introduced by Tomotika (1935) and studied for special cases by Chandrasekhar (1961) and for limiting cases by Lee and Flumerfelt (1981). The effects of vorticity and the continuity of the tangential component of velocity and stress cannot be enforced in the frame of potential flow of a viscous fluid, but the extensional effects of viscous stresses on capillary collapse are retained in the normal stress balance.

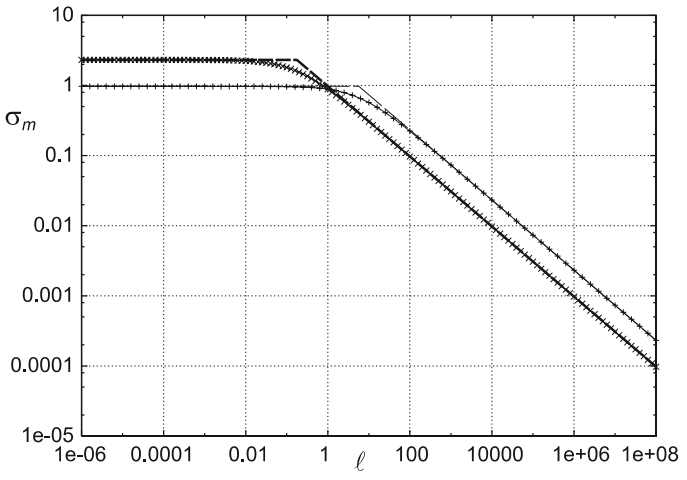

(a) σ_{mI} versus ℓ

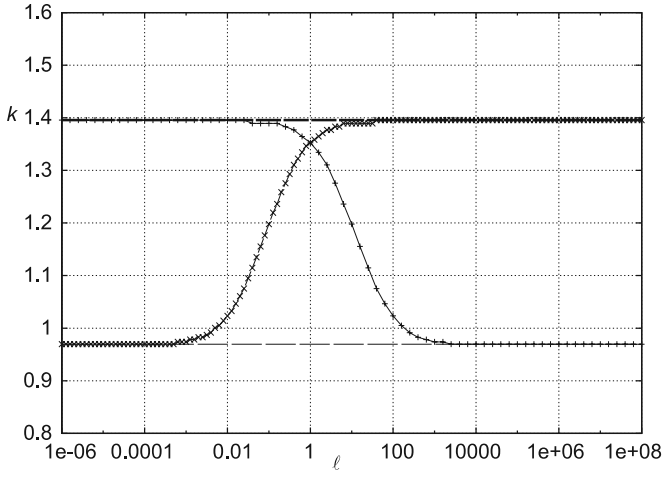

(b) k_{mI} versus ℓ

Fig. 16. Maximum growth rate σ_{mI} and associated wave number for IPF: $+++$ fluid ℓ is inside, $\times\times\times$ fluid is outside. σ is made dimensionless with $T_{\mathrm{l}} = D/\sqrt{\gamma/\rho_{\mathrm{l}}D}$ when fluid ℓ is inside and with $T_{\mathrm{l}} = D/\sqrt{\gamma/\rho_{\mathrm{a}}D}$ when it is outside. The asymptotic forms (5.2) and (5.3) are marked with a dashed line and bold dashed line respectively.

Analysis of the viscous flow reveals the existence of finite maximum values of k_{m}, for certain viscosity ratios, as J is increased (Figs. 9 and 10). We found that IPF emerges as a unique high Reynolds limit (practically, with $J > \mathrm{O}(10)$) of both the fully viscous and viscous potential flow analysis. The inviscid limit depends only on the density ratio ℓ.

Comparisons of growth rate curves for fully viscous flow, viscous potential flow and IPF are given in Figs. 2–8 for 7 of 28 fluid pairs. Comparisons of the maximum growth rate σ_{m} and associated wavenumber k_{m} as a function of $\sqrt{J}$ for different values of m and ℓ are presented in Figs. 11–15. From these figures we may conclude that the maximum growth rates and wavenumber for IPF, viscous potential flow and fully viscous flow converge when J is large; for smaller J, the

growth rates of IPF are greatest (and independent of J) and these fully viscous flows are smallest and decrease with decreasing J. The growth rates of viscous potential flow track fully viscous flow and lie between IPF and fully viscous flow. A similar behavior is exhibited by the associated wavenumbers, with viscous potential flow giving the smallest k_m and IPF the largest k_m when $\sqrt{J}$ is not too large.

It follows, from the comparisons just presented, that viscous potential flow is a much better approximation of fully viscous flow than IPF for small J and no worse than IPF for all J. There is absolutely no advantage to putting the viscosities to zero in the analysis of potential flow.

The convergence of fully viscous flow and viscous potential flow to IPF when the Reynolds number J is large could have been anticipated from general fluid mechanical principles. On the other hand, Harper (1972) has argued (see also Joseph and Liao, 1994, pp. 6 and 7) that the success of the Levich (1949) potential flow approximation in calculating the drag on a rising spherical bubble of gas is due to the nature of the boundary layer at a tangentially stress-free surface. Presumably liquid–gas surfaces approximate such stress free conditions when the viscosity contrast is large, but not at liquid–liquid surfaces like water and benzene in which the viscosities are comparable.

Levich computed the drag by equating $U_r D_r$, where U_r is the rise velocity and D_r the drag, to the viscous dissipation in the liquid as would be true for the steady drag on a solid. The approximation arises on both sides of the balance, on the left side—either by assuming that every part of the boundary of the bubble moves with the same velocity U_r, or that the tangential component of the traction vector vanishes at the bubble's surface—and on the right, by evaluating the dissipation integral on potential flow over a sphere (see Joseph et al., 1993).

Our calculations of capillary instability given here show that viscous potential flows approximate fully viscous liquid–liquid as well as gas–liquid flows in cases in which IPF fails dismally provided only that J is not too small.

Acknowledgements

This work was supported by the NSF/CTS-0076648, the Engineering Research Program of the Office of Basic Energy Sciences at the DOE and by an ARO grant DA/DAAH04.

References

Chandrasekhar, S., 1961. Hydrodynamic and Hydromagnetic Stability. Oxford University Press, Oxford.

Funada, T., Joseph, D.D., 2001. Viscous potential flow analysis of Kelvin–Helmholtz instability in a channel. J. Fluid Mech. 445, 263–283.

Harper, J.F., 1972. The motion of bubbles and drops through liquids. Adv. Appl. Mech. 12, 59–129.

Joseph, D.D., Belanger, J., Beavers, G.S., 1999. Breakup of a liquid drop suddenly exposed to a high-speed airstream. Int. J. Multiphase Flow 25, 1263–1303.

Joseph, D.D., Liao, T.Y., 1994. Potential flows of viscous and viscoelastic fluids. J. Fluid Mech. 265, 1–23.

Joseph, D.D., Liao, T.Y., Hu, H.H., 1993. Drag and moment in a viscous potential flow. Eur. J. Mech. B/Fluids 12, 97–106.

Joseph, D.D., Beavers, G.S., Funada, T., 2002. Rayleigh–Taylor instability of viscoelastic drops at high Weber numbers. J. Fluid Mech. 453, 109–132.

Lee, W.K., Flumerfelt, R.W., 1981. Instability of stationary and uniformly moving cylinderical fluid bodies. I. Newtonian systems. Int. J. Multiphase Flow 7, 363–383.

Levich, V.G., 1949. The motion of bubbles at high Reynolds numbers. Zh. Eksperim Teor. Fiz. 19, 18, see also Physiochemical Hydrodynamics, English translation by Scripta Technica, Prentice-Hall, Englewood Cliffs, NJ, 1962, p. 436ff.

Plateau, 1873. Statique experimentale et theorique des liquide soumis aux seules forces moleculaire, vol ii, 231.

Rayleigh, L., 1879. On the capillary phenomena of jets. Proc. Roy. Soc. London A 29, 71–79.

Rayleigh, L., 1892. On the instability of a cylinder of viscous liquid under capillary force. Phil. Mag. 34, 145–154.

Tomotika, S., 1935. On the instability of a cylindrical thread of a viscous liquid surrounded by another viscous fluid. Proc. Roy. Soc. London A 150, 322–337.

Weber, C., 1931. Zum Zerfall eines Flüssigkeitsstrahles. Ztschr. f. angew. Math. und Mech. 11, 136–154.